Electron-capture decay rate of ^{7}Be@C_{60} by first-principles calculations based on density functional theory

Tsuguo Morisato
Accelrys K.K., Nishishinbashi TS Building, 11F, 3-3-1 Nishishinbashi, Minato-ku, Tokyo 105-0003, Japan

Kaoru Ohno
Department of Physics, Yokohama National University, 79-5 Tokiwadai, Hodogaya-ku, Yokohama 240-8501, Japan

Tsutomu Ohtsuki and Kentaro Hirose
Laboratory of Nuclear Science, Tohoku University, 1-2-1 Mikamine, Taihaku-ku, Sendai 982-0826, Japan

Marcel Sluiter
Department of Materials Science and Engineering, Delft University, Stevinweg 1, 2628 CN Delft, Netherlands

Yoshiyuki Kawazoe
Institute for Materials Research, Tohoku University, 2-1-1 Katahira, Aoba-ku, Sendai 980-8577, Japan
(Received 7 June 2008; published 23 September 2008)

Carrying out a first-principles calculation assuming linear relationship between the electron density at Be nucleus and the electron-capture (EC) decay rate, we explained why ^{7}Be@C_{60} shows higher EC decay rate than ^{7}Be crystal, which was originally found experimentally by Ohtsuki *et al.* [Phys. Rev. Lett. **93**, 112501 (2004)]. From the results of the calculation, we found that there are inequivalent four stable (i.e., lower energy) Be sites inside C_{60} and that center of C_{60} (C_C_{60}) is the most favorable site. For C_C_{60}, the electron density at the Be nucleus is the highest. It is also much higher than that at the Be nucleus in a Be crystal. Also, we estimated the expected electron density at the Be nucleus at room temperature by taking statistical average of the electron densities at the four Be nucleus sites using the Boltzmann distribution. The results of the calculation show fairly good agreement with the experimental results. In this paper, we focus on the detail of calculation, which was not fully demonstrated in the paper by Ohtsuki.

DOI: 10.1103/PhysRevB.78.125416 PACS number(s): 71.20.Tx, 61.72.up, 23.40.−s

I. INTRODUCTION

Since Kroto *et al.* discovered the C_{60} molecule,[1] many scientists have been interested in the novel properties of this new material. One of the most attractive features is that C_{60} can encapsulate another atom. It is interesting to study the new properties of the cluster, M@C_{60}, and how the atom behaves inside C_{60}. So far, many works have been devoted to this subject.[2–10]

Recently, Ohtsuki *et al.* measured the electron-capture (EC) decay rate of the ^{7}Be nucleus inserted inside the C_{60} cage.[9,10] The EC decay reaction can be written as

$$p + e^{-} \rightarrow n + \nu_e, \tag{1}$$

where p, e^{-}, n, and ν_e are proton, electron, neutron, and neutrino, respectively. A ^{7}Be atom decays to ^{7}Li by electron capture (EC). As first suggested by Segré *et al.*,[11–13] the EC decay rate depends on the density of atomic electrons at the nuclear site. Assuming a linear relation between decay rate and electron density, we expect that the EC decay rate is proportional to the electron density at the Be nucleus. External factors such as chemical forms and pressure may alter the electron density at the nucleus and thus affect the EC decay rate. In recent studies, there have been several observations or calculations concerning the change in half-life according to the host materials,[14–18] chemical forms,[19–22] and pressure.[23,24] Although, in most of these environments, the half-life is longer than 53.10 days, Ohtsuki *et al.* found that the half-life of ^{7}Be@C_{60} is 52.65 ± 0.04 days at room temperature (RT) (293 K) and moreover 52.47 ± 0.04 days at liquid-helium temperature (5 K).[9,10] This result shows that the chemical environment inside C_{60} drastically changes the electronic density at the Be nucleus and that the temperature may also affect the electronic density at the Be nucleus. In this paper, we discuss the EC decay rate of ^{7}Be@C_{60} by carrying out a first-principles calculation for the electronic density at the Be nucleus inside C_{60} on the basis of the density functional theory (DFT).

II. CALCULATION METHOD

In order to express correctly the cusp-like profile of the electron density near the nucleus, we use the all-electron first-principles calculation program, DMol^3.[25,26] It adopts a linear combination of the atomic orbital (LCAO) method and the numerical localized orbitals as basis functions. This basis set is appropriate for expressing such cusp-like profile of the electron density near the nucleus. For the exchange-correlation energy, we employed the BLYP method, which combines the exchange functional due to Becke[27] with the correlation functional of Lee-Yang-Parr.[28] In DMol^3, basis functions are given numerically as values on an atomic-centered spherical-polar mesh, rather than as analytical functions (e.g., Gaussian orbitals). The angular portion of each

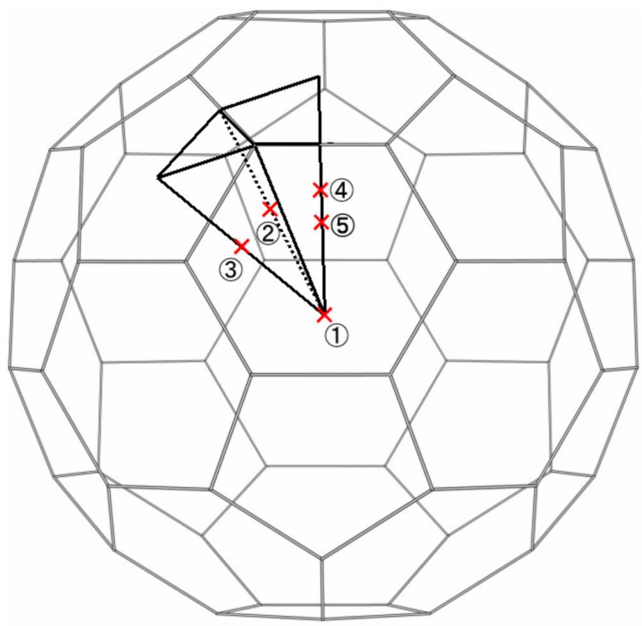

FIG. 1. (Color online) Irreducible region of C_{60} by point-group operations. The crosses and numbers correspond to the candidates of stable Be sites shown in Fig. 2.

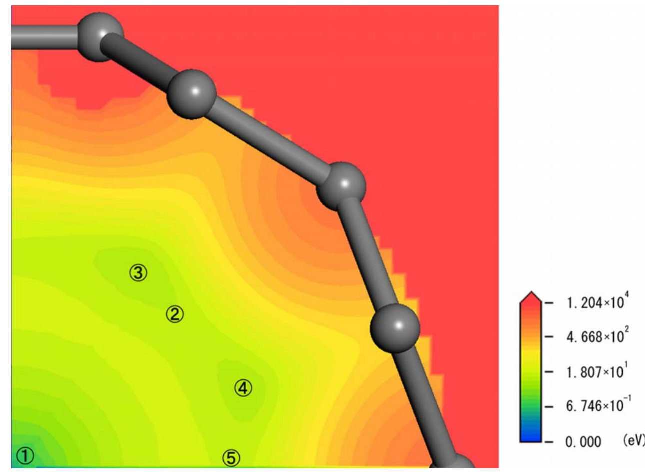

FIG. 2. (Color online) Total energy contour map of Be@C_{60} with respect to the position of a Be atom. The points denoted with circled numbers from 1 to 5 correspond to center of C_{60} (C_C_{60}), under the center of a single bond (U_sb), under the center of a five-membered ring (U_5), under the center of a six-membered ring (U_6), and under the center of a double bond (U_db), respectively. Each point is also shown in Fig. 1.

function is the appropriate spherical harmonic functions. The radial portion is obtained by solving the atomic DFT equations numerically. Therefore, even only one function has important information in numerical basis set, while only one function in analytical basis set has less meaning as an atomic orbital. In the present work, we used the double-numeric quality basis set with polarization functions (DNP). The size of the DNP basis set is comparable to Gaussian 6−31G**. However, the numerical basis set is much more accurate than a Gaussian basis set of the same size as demonstrated above.

III. RESULTS AND DISCUSSION

A. Be@C_{60} at 0 K

At first, we explored the most stable sites of Be in a C_{60} cage. For this purpose, we carried out single point energy calculations varying the Be site on a high symmetry plane inside C_{60}. C_{60} has the point group, I_h, i.e., the full icosahedral symmetry, which has 120 point-group operations. In Fig. 1, an irreducible region of I_h in C_{60} is shown. High symmetric triangles constructing this region except surface of C_{60} can be unfolded into one sheet of plane across high symmetric points such as the center of C_{60}, the centers of five- and six-membered rings, and the centers of single and double bonds. So, the calculations were done for the 962 Be sites, which are grid points on that plane. We excluded points outside C_{60} and those which are too close to carbon atom, i.e., less than 0.5 Å.

Total energies calculated for those Be sites are plotted to draw a contour map of the potential energy that Be atom feels in Fig. 2. From this result, we see that there are inequivalent five points as candidates for local minima of Be sites: center of C_{60} (C_C_{60}), under the center of a five-membered ring (U_5), under a six-membered ring (U_6), under the center of a single bond (U_sb), and under the center of a double bond (U_db). Among these five points, U_sb and U_db may not seem to be local minima in the contour map. However, we took them as candidates of stable Be sites from the viewpoint of symmetry. The corresponding five points in the irreducible region of C_{60} are shown also in Fig. 1.

The geometry of C_{60} was then optimized for the five stable sites (C_C_{60}, U_5, U_6, U_sb, and U_db) to make sure whether those five Be sites are really stable. The results are shown in Table I. A part of the data presented in Table I is taken from our previous paper.[10] From Table I, one can see that the most stable position of the Be atom inside the C_{60} cage is C_C_{60} among all the cases investigated in the present

TABLE I. Total energy difference measured from the most stable structure C_C_{60} (eV), spin magnetic moment (μ_B), and electron density at Be nucleus (e^-/a_B^3) for the systems, C_C_{60}, U_sb, U_5, U_6, U_db, Be atom, and Be crystal. Here, a_B denotes the Bohr radius. A part of the data is taken from our previous paper (Ref. 10).

	Total energy difference (eV)	Spin magnetic moment (μ_B)	Electron density at Be nucleus (e^-/a_B^3)
C_C_{60}	0.000	0.0	36.016
U_sb	0.098	0.0	35.243
U_5	0.068	2.0	35.287
U_6	0.142	2.0	35.332
U_db	0.309	2.0	35.377
Be atom		0.0	35.954
Be crystal		0.0	35.423

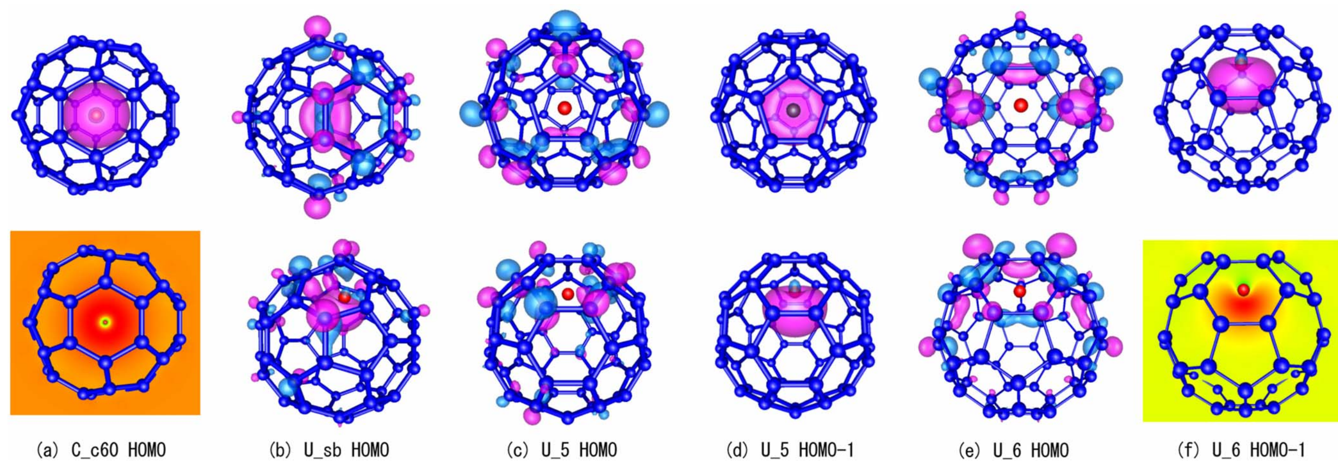

FIG. 3. (Color online) Isosurface plots and contour maps of the HOMO and HOMO-1 levels for four Be sites: (a) HOMO of C_C_{60}, (b) HOMO of U_sb, (c) HOMO of U_5, (d) HOMO-1 of U_5, (e) HOMO of U_6, and (f) HOMO-1 of U_6. The upper and lower figures of (b)–(e) are the views from different angles. These figures are taken from Ref. 10.

calculation. For U_5, U_6, and U_db sites, the system shows 2.0 μ_B spin magnetic moment. U_db shows very large total energy compared to other sites, so we decide to discard it from the candidates.

We plot the highest occupied molecular orbital (HOMO) for each Be site in Fig. 3 to see the difference in the electronic structure among these four Be sites except U_db. Since we already posted this figure in the previous report,[10] we discuss this briefly here. From this figure, we can see that only the case of C_C_{60} has an orbital localized around the Be atom just like an isolated atom. For the case of U_sb, the Be2s and t_{1u} [the lowest unoccupied molecular orbital (LUMO) of C_{60}] form bonding and antibonding orbitals. The bonding orbital and the antibonding orbitals become HOMO and LUMO, respectively. For U_5 and U_6 sites, HOMO and the second highest occupied molecular orbital (HOMO-1) have the same spin direction. In these two cases, Be atom is close to a five- or six-membered ring, and one of the Be2s electrons moves to t_{1u}, flipping the spin direction. Since one electron at the HOMO level, i.e., t_{1u}, spreads over a large area of C_{60} while the other electron remaining at the Be2s state is confined only in a small region around Be atom, there is an energy gain by the triplet spin configuration due to the exchange interaction.

As side products of these geometry optimizations, we could obtain the electron density at each Be nucleus site. In addition to the inequivalent four Be sites inside C_{60}, we carried out the all-electron calculation also for a free Be atom and for Be metal to determine their electron densities at the Be nucleus. For Be metal, we carried out structural optimization also. The Be crystal is hexagonal and two Be atoms exist in a primitive unit cell. In the optimization, we took $18\times18\times12$ $\boldsymbol{k}$ points. The results of the electron density at the Be nucleus for all these systems are also shown in Table I. Among all these results, C_C_{60} has the largest value. It is even larger than that of a free Be atom. This is because the Be2s electrons are closely confined in C_{60} and have higher amplitude at the Be nucleus. If we compare the density at the other three sites of Be inside C_{60} (except for C_C_{60}) and in the Be metal, we find that the density is higher in the Be metal than at the other three sites inside C_{60}. In the Be metal, the tails of Be2s electrons spread from the adjacent Be atoms are superposed at the Be nucleus. In contrast, there is only one Be atom in U_5, U_6, and U_sb, and the Be2s electrons spread into whole C_{60}. Since there is no overlap from other Be2s electrons like the Be metal, the electron density at U_5, U_6, and U_sb is less than that in the Be metal.

To confirm the charge transfer, we plotted the difference in the charge density distribution for U_5, C_C_{60}, and Be metal. The differences in the charge density distributions are defined here by

$$\rho_{\mathrm{diff}}(\boldsymbol{r}) = \rho_{\mathrm{Be@C_{60}}}(\boldsymbol{r}) - [\rho_{\mathrm{C_{60}}}(\boldsymbol{r}) + \rho_{\mathrm{Be\_atom}}(\boldsymbol{r})] \qquad (2)$$

or,

$$\rho_{\mathrm{diff}}(\boldsymbol{r}) = \rho_{\mathrm{Be\_metal}}(\boldsymbol{r}) - \rho_{\mathrm{Be\_atom}}(\boldsymbol{r}), \qquad (3)$$

where $\rho_{\mathrm{C_{60}}}(\boldsymbol{r})$, $\rho_{\mathrm{Be\_atom}}(\boldsymbol{r})$, $\rho_{\mathrm{Be@C_{60}}}(\boldsymbol{r})$, and $\rho_{\mathrm{Be\_metal}}(\boldsymbol{r})$ are the electronic charge densities at $\boldsymbol{r}$ for C_{60}, free Be atom, Be@C_{60}, and Be metal, respectively.

In Fig. 4, the $\rho_{\mathrm{diff}}(\boldsymbol{r})$ is shown in color. For the case of Be@C_{60}, the red or blue regions show the areas in which electronic charge density increases or decreases, respectively, compared to the charge density given by the superposition of a Be atom and C_{60}. As for the Be metal, the red or blue regions have almost the same meaning as those of Be@C_{60}, but the comparison is done against the charge density given by the superposition of Be atoms. From this figure, we can easily make sure that the charge density at the Be nucleus of C_C_{60} is larger than that of a free Be atom. On the contrary, for the cases of Be metal and U_5, it is clear that the electronic charge around the Be nucleus goes outside and the density at the Be nucleus decreases.

Figure 5 shows experimentally measured half-lives of the EC decay for several systems.[10] According to these experimental results, one can see that the EC decay rate of ^{7}Be@C_{60} at 5 K is the fastest. This experimental result suggests that ^{7}Be@C_{60} at 5 K has the largest electron density at Be nucleus. This is certainly consistent with the present (computational) result telling that C_C_{60} is the most stable

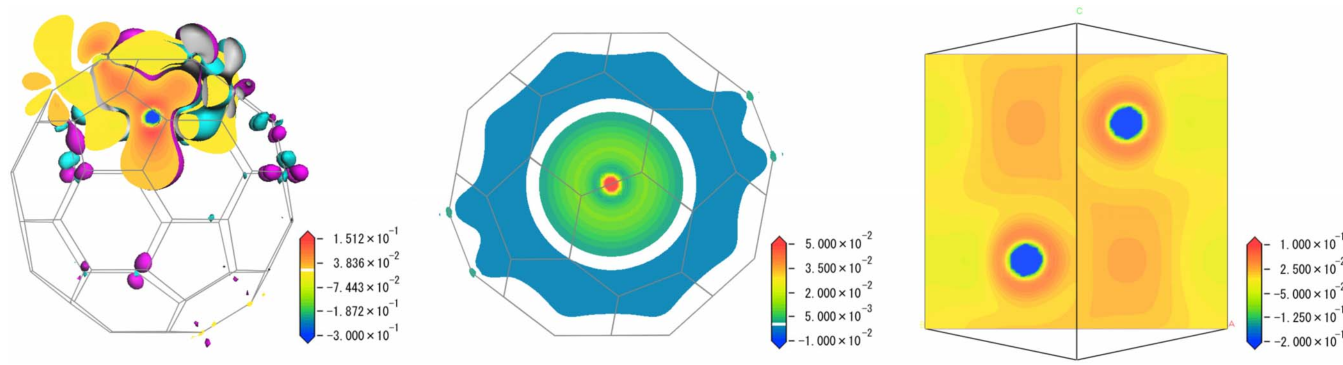

FIG. 4. (Color online) Contour map of electron density differences defined by Eq. (2) for the case of U_5 (left) and C_C_{60} (center) and by Eq. (3) for the case of Be metal (right). In these figures, the area including zero is excluded. In the case of U_5, to show that the Be2s electron transfers in large area of C_{60}, the isosurfaces having the value +0.01 $e^-/Å^3$ and −0.01 $e^-/Å^3$ are also plotted in pink and light blue, respectively. The unit of values on the color bars is $e^-/Å^3$.

Be site inside C_{60} at the absolute zero temperature and its electron density at the Be nucleus is the largest among four low-energy Be sites inside C_{60}.

B. Be@C_{60} at room temperature

As we mentioned above, the EC decay rate of ^{7}Be@C_{60} is higher at 5 K than at RT. We showed C_C_{60} is the most preferable Be position at 0 K in Sec. III A. At RT, Be atoms perform ratchet motion among stable Be sites inside C_{60}. Although energy barrier from C_C_{60} to other sites may be high to pass through, the hopping should occur during a very long time scale of real measurement such as more than 160 days in the experiment.[10] Here, we estimate the probability of finding a Be atom at each site at RT by assuming the Boltzmann distribution and estimate the expected electron density at the Be nucleus at RT by taking the statistical average of the electron densities at different Be positions. That is, using the total energy $E(\boldsymbol{r})$ and the electron density $\rho(\boldsymbol{r})$ calculated at each Be position $\boldsymbol{r}$ inside the C_{60} cage, we can evaluate the statistical average of the electron density at the Be nucleus at temperature T according to the Boltzmann distribution with the Be nucleus position $\boldsymbol{r}$ as follows:

$$\langle \rho(\boldsymbol{r}) \rangle = \frac{\int \rho(\boldsymbol{r}) \exp\left[-\frac{E(\boldsymbol{r})}{k_B T}\right] d\boldsymbol{r}}{\int \exp\left[-\frac{E(\boldsymbol{r})}{k_B T}\right] d\boldsymbol{r}}. \quad (4)$$

Here, k_B is the Boltzmann constant. Expanding $E(\boldsymbol{r})$ around each local minimum position $\boldsymbol{r}_i=(x_i,y_i,z_i)$ in a quadratic form as $E(\boldsymbol{r}) \sim E(\boldsymbol{r}_i)+a_i(x-x_i)^2+b_i(y-y_i)^2+c_i(z-z_i)^2$, we readily evaluate the local integration around $\boldsymbol{r}_i$ to be

$$\int_{\text{around } \boldsymbol{r}_i} \exp\left[-\frac{E(\boldsymbol{r})}{k_B T}\right] d\boldsymbol{r} \sim \sqrt{\frac{(\pi k_B T)^3}{a_i b_i c_i}} \exp\left[-\frac{E(\boldsymbol{r}_i)}{k_B T}\right]. \quad (5)$$

Moreover, we write the number of equivalent positions as α_i. Since C_{60} is highly symmetric (with the I_h symmetry), there are α_i=20, 12, and 30 equivalent positions for U_6 (i=2), U_5 (i=3), and U_sb (i=4), respectively. (Obviously α_1 =1 at C_C_{60}.) Therefore the expression for the average density is given by

$$\langle \rho(\boldsymbol{r}) \rangle \sim \frac{\sum_{i=1}^{4} \rho(\boldsymbol{r}_i) \frac{\alpha_i}{\sqrt{a_i b_i c_i}} \exp\left[-\frac{E(\boldsymbol{r}_i)}{k_B T}\right]}{\sum_{i=1}^{4} \frac{\alpha_i}{\sqrt{a_i b_i c_i}} \exp\left[-\frac{E(\boldsymbol{r}_i)}{k_B T}\right]}. \quad (6)$$

In reality, due to the asymmetry, the coefficients of the plus and minus directions for quadratic form of $E(\boldsymbol{r})$ are different, and a slight modification of Eq. (6) is necessary. Consequently, the final expression for the average density at finite temperature is given by

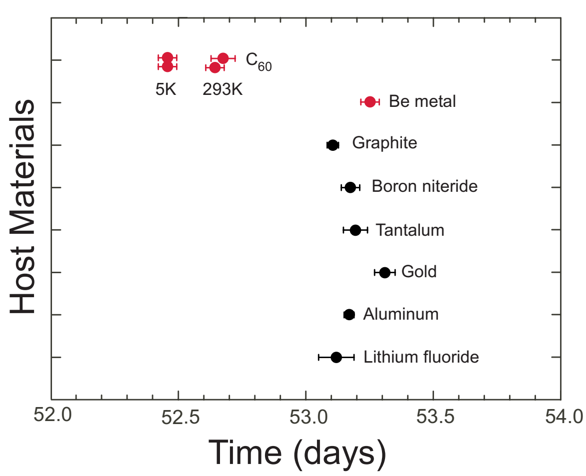

FIG. 5. (Color online) Half-lives experimentally measured at liquid-helium temperature (T=5 K) and at room temperature (RT) (T=293 K) for the samples of ^{7}Be@C_{60}, and of ^{7}Be in Be metal at RT in this study (red) (Refs. 9 and 10). Two dots in each temperature of ^{7}Be@C_{60} show that two separate measurements were carried out in order to confirm reproducibility. The half-lives of ^{7}Be in other materials [boron nitride, graphite, tantalum, gold (Ref. 17), aluminum (Ref. 22), and lithium fluoride (Ref. 14)] given in the literatures are also shown for comparison (black). The error bar at each dot shows the statistical error in one measurement.

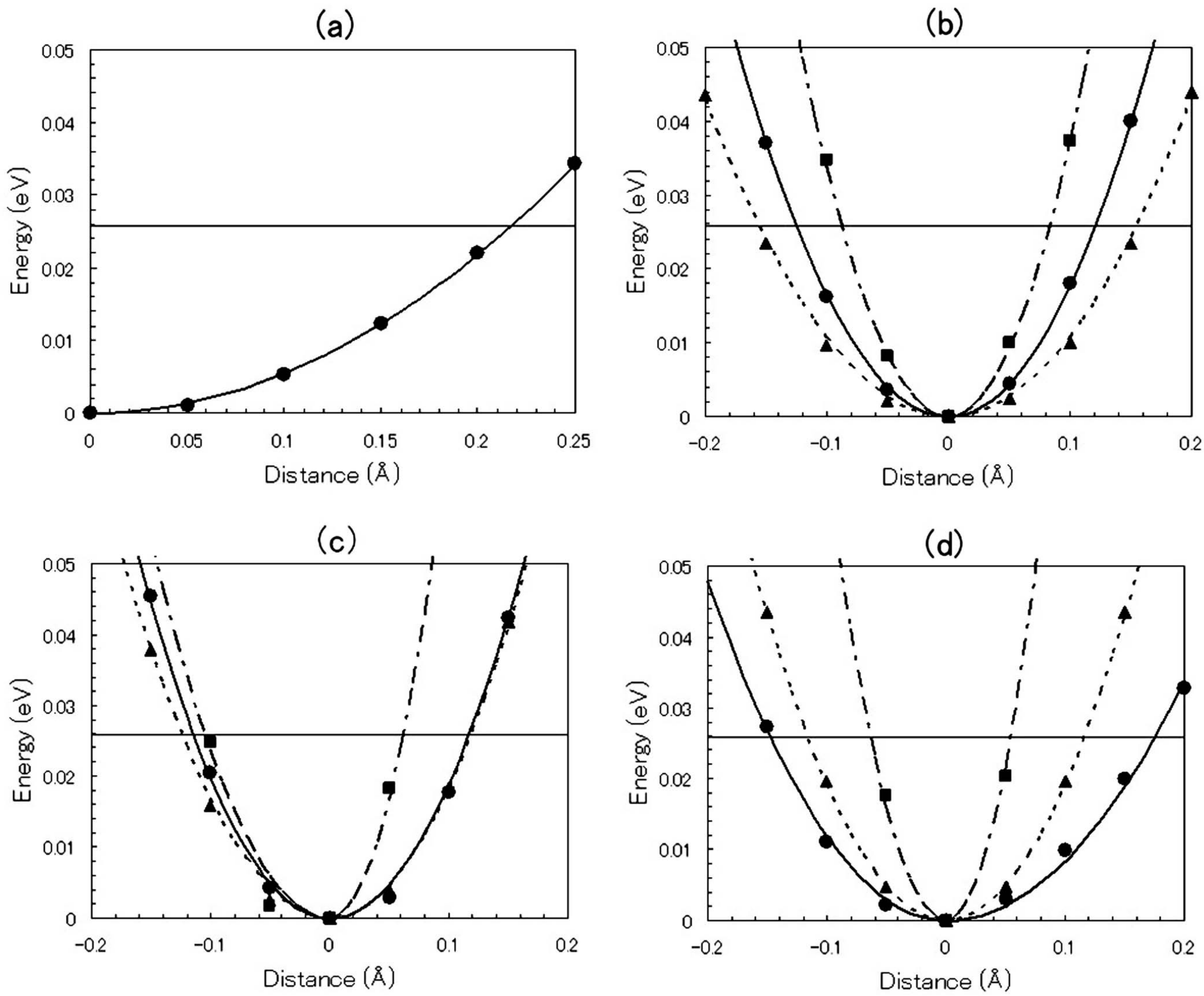

FIG. 6. Total energy differences from each local minimum of Be in C_{60} along x, y, and z axis are plotted as dots of circle (x), triangle (y), and square (z), respectively. Four graphs, i.e., (a), (b), (c), and (d), correspond to C_C_{60}, U_6, U_5, and U_sb, respectively. The quadratic functions fitted to these points are also plotted as line, dotted line, and dashed-dotted line for x, y, and z directions, respectively. The horizontal line shows the energy corresponding to RT (293 K).

$$\langle\rho(\boldsymbol{r})\rangle \sim \frac{\sum_{i=1}^{4}\rho(\boldsymbol{r}_i)\alpha_i \exp\left[-\frac{E(\boldsymbol{r}_i)}{k_BT}\right]\sum_{l,m,n=1}^{2}\sqrt{(a_{il}b_{im}c_{in})^{-1}}}{\sum_{i=1}^{4}\alpha_i \exp\left[-\frac{E(\boldsymbol{r}_i)}{k_BT}\right]\sum_{l,m,n=1}^{2}\sqrt{(a_{il}b_{im}c_{in})^{-1}}}, \tag{7}$$

where l, m, and n, which are 1 or 2, represent plus or minus direction of x, y, and z, respectively. To obtain the potential coefficients around each local minimum position, i.e., a_{i+}, a_{i-}, b_{i+}, b_{i-}, c_{i+}, c_{i-}, total energies of $Be@C_{60}$ were calculated, changing Be positions little by little (0.05 Å each) and plotted and fitted in quadratic functions. In these calculations, each system was rotated so that the line across the center of C_{60} and each local minimum is along z axis. The total energies and the fitted quadratic functions around each local minimum position are shown in Fig. 6. The obtained potential coefficients are listed in Table II. In the graphs of Fig. 6, the energy corresponding to RT (1 eV=11600 K) is expressed as a horizontal line, and each quadratic curve crosses this line at short distance, which is less than 0.2 Å except C_C_{60}. This implies that the energies of transition states from one site to other sites are quite high for Be to pass through at RT within a short time and Be may stay around one site for a long time at RT in thermal equilibrium state.

At absolute zero temperature (T=0), the Be atom is located at C_C_{60} and the electron density at the Be nucleus is equal to 36.016 e^-/a_B^3, while at the room temperature, it is estimated to be 35.899 e^-/a_B^3 from Eq. (7). Here, a_B denotes the Bohr radius. The relative difference between them amounts to 0.33%, which should be compared with the relative difference 0.34% of the experimentally determined half-

TABLE II. Potential coefficients (eV/Å^2), which are derived from the total energy calculation, changing the Be location from each stable point slightly to positive and negative directions along each Cartesian coordinate axis.

	Potential coefficients (eV/Å^2)					
	a_{i+}	a_{i-}	b_{i+}	b_{i-}	c_{i+}	c_{i-}
C_C_{60}	0.545	0.545	0.545	0.545	0.545	0.545
U_6	1.773	1.657	1.081	1.074	3.752	3.377
U_5	1.891	1.982	1.836	1.689	6.740	2.365
U_sb	0.843	1.195	1.921	1.921	8.765	6.431

lives (52.47 ± 0.04 days at liquid-helium temperature and 52.65 ± 0.04 days at room temperature). On the other hand, if we compare the electron density of Be@C_{60} at RT (35.899 e^-/a_B^3) with that of Be metal at absolute zero temperature (35.423 e^-/a_B^3), the relative difference between them amounts to 1.3%. This value should be compared with the relative difference 1.1% of the experimentally determined half-lives (52.65 ± 0.04 days for ^{7}Be@C_{60} and 53.25 ± 0.04 days for Be metal at RT). The agreement between the theory and the experiment is fairly good. According to the present calculation, the EC decay rate of ^{7}Be in C_{60} at absolute zero temperature is about 1.67% faster than that of ^{7}Be in Be metal at absolute zero temperature, which is surprisingly a very big change in the half-life.

By means of the method adopted here, it is basically possible to calculate theoretically the "averaged" electron density at the ^{7}Be nucleus at any temperature. That is, we succeeded in representing the temperature dependence of the averaged electron density at the ^{7}Be nucleus by analytical formula using the Boltzmann distribution with Be position. In the present study, we should take very long experimental time scales into account, and thermal equilibrium would be totally achieved. It is intriguing to investigate experimentally more precise temperature dependence (e.g., at $T=20$ K, 40 K, 60 K, etc.) of the EC decay rate. Such an investigation is, however, left for a future study.

IV. CONCLUSION

In this paper, we have explained by means of a first-principles calculation why ^{7}Be@C_{60} shows a higher EC decay rate than ^{7}Be crystal, which was originally found experimentally by Ohtsuki *et al.*[9,10] We found that there are inequivalent four stable Be sites inside C_{60} and that center of C_{60} (C_C_{60}) is the most favorable site. For C_C_{60}, we showed that the electron density at the Be nucleus is the highest among these Be sites and also higher than Be metal. Since valence electrons of Be are closely confined inside C_{60}, the electron density at the Be nucleus has a relatively large value for C_C_{60}. Also, we estimated expected electron density at the Be nucleus at room temperature by statistical calculation including total energies and the electron densities at various Be nucleus positions. The results of our calculation are in fairly good agreement with the experimental results.

ACKNOWLEDGMENTS

This work was supported by the Grant-in-Aid for Scientific Research C (Grants No. 10640535 and 12640532) and Scientific Research B (Grants No. 17310067 and 17350024), and Scientific Research on Priority Areas (Grants No. 18036005 and 19019005) from the Japan Society for the Promotion of Science and from the Ministry of Education, Culture, Sports, Science and Technology of Japan. This research was also supported by the REIMEI Research Resources of JAERI, and the Mitsubishi Foundation.

[1] H. W. Kroto, J. R. Health, S. C. O'Brien, R. F. Curl, and R. E. Smalley, Nature (London) **318**, 162 (1985).

[2] H. Funasaka, K. Sugiyama, K. Yamamoto, and T. Takahashi, J. Phys. Chem. **99**, 1826 (1995).

[3] M. D. Diener and J. M. Alford, Nature (London) **393**, 668 (1998).

[4] O. V. Boltalina, N. Ioffe, I. D. Sorokin, and L. N. Sidorov, J. Phys. Chem. A **101**, 9561 (1997).

[5] J. Lu, X. Zhang, and X. Zhao, Chem. Phys. Lett. **312**, 85 (1999).

[6] J. Lu, Y. Zhou, X. Zhang, and X. Zhao, Chem. Phys. Lett. **352**, 8 (2002).

[7] T. Ohtsuki, K. Masumoto, K. Ohno, Y. Maruyma, Y. Kawazoe, K. Sueki, and K. Kikuchi, Phys. Rev. Lett. **77**, 3522 (1996).

[8] T. Ohtsuki and K. Ohno, in *Clusters and Nonomaterials*, edited by Y. Kawazoe, T. Kondow, and K. Ohno, Springer Series in Cluster Physics (Springer-Verlag, Berlin, 2002) Chapter 7, p. 171.

[9] T. Ohtsuki, H. Yuki, M. Muto, J. Kasagi, and K. Ohno, Phys. Rev. Lett. **93**, 112501 (2004).

[10] T. Ohtsuki, K. Ohno, T. Morisato, T. Mitsugashira, K. Hirose, H. Yuki, and J. Kasagi, Phys. Rev. Lett. **98**, 252501 (2007).

[11] E. Segré, Phys. Rev. **71**, 274 (1947).

[12] E. Segré and C. E. Wiegand, Phys. Rev. **75**, 39 (1949).

[13] R. F. Leininger, E. Segré, and C. Wiegand, Phys. Rev. **76**, 897 (1949).

[14] M. Jaeger, S. Wilmes, V. Kolle, G. Staudt, and P. Mohr, Phys.

Rev. C **54**, 423 (1996).
[15] A. Ray, P. Das, S. K. Sasha, S. K. Das, B. Sethi, A. Mookerjee, C. B. Chaudhuri, and G. Pari, Phys. Lett. B **455**, 69 (1999).
[16] A. Ray, P. Das, S. K. Sasha, and S. K. Das, Phys. Lett. B **531**, 187 (2002).
[17] E. B. Norman, G. A. Rech, E. Browne, R. M. Larimer, M. R. Dragowsky, Y. D. Chan, M. C. P. Isaac, R. J. McDonald, and A. R. Smith, Phys. Lett. B **519**, 15 (2001).
[18] Z. Y. Liu, C. B. Li, S. G. Wang, J. Zhou, Q. Y. Meng, S. J. Lu, and S. H. Zhou, Phys. Lett. **20**, 829 (2003).
[19] C. A. Huh, Earth Planet. Sci. Lett. **171**, 325 (1999).
[20] H. W. Johlige, D. C. Aumann, and H. J. Born, Phys. Rev. C **2**, 1616 (1970).
[21] J. A. Tossell, Earth Planet. Sci. Lett. **195**, 131 (2002).
[22] F. Lagoutine, J. Legrand, and C. Bac, Int. J. Appl. Radiat. Isot. **26**, 131 (1975).
[23] W. K. Hensley, W. A. Bassett, and J. R. Huizenga, Science **181**, 1164 (1973).
[24] L. Liu and C. A. Huh, Earth Planet. Sci. Lett. **180**, 163 (2000).
[25] B. Delley, J. Chem. Phys. **92**, 508 (1990).
[26] B. Delley, J. Chem. Phys. **113**, 7756 (2000).
[27] A. D. Becke, J. Chem. Phys. **88**, 2547 (1988).
[28] C. Lee, W. Yang, and R. G. Parr, Phys. Rev. B **37**, 785 (1988).